Investigation of E-Divertor Plasma during Simultaneous Injection of Hydrogen and Impurity Gases into GAMMA 10/PDX by Using the LINDA Code*)

Md. Shahinul ISLAM, Yousuke NAKASHIMA, Akiyoshi HATAYAMA[1)], Kazuya ICHIMURA[2)], Takaaki IIJIMA, Md. Maidul ISLAM, Takayuki YOKODO, Guanyi LEE, Tsubasa YOSHIMOTO, Sotaro YAMASHITA, Naomichi EZUMI and Mizuki SAKAMOTO

Plasma Research Center, University of Tsukuba, Tsukuba, Ibaraki 305-8577, Japan
[1)]*Graduate School of Science and Technology, Keio University, Hiyoshi, Yokohama 223-8522, Japan*
[2)]*Graduate School of Engineering, Kobe University, Kobe, Hyogo 657-8501, Japan*

(Received 26 December 2017 / Accepted 21 May 2018)

This paper describes the behavior of plasma parameters in the E-divertor region of GAMMA 10/PDX numerically by using the multi-fluid code (LINDA) during injection of hydrogen (H) and Argon (Ar). A remarkable reduction in the electron temperature (T_e) has been recognized due to Ar injection. For only Ar 6.0×10^{17} m^{-3} injection, T_e on the target plate decreases to nearly 10 eV. T_e also reduces according to the increment of H injection. The ion temperature (T_i) on the target plate also decreases according to the increment of injected H neutral density. A tendency of saturation in the particle flux and the electron density is observed at the higher H injection in the case of simultaneous injection of H and Ar. The charge exchange loss enhances significantly during H injection. The radiation power loss also enhances for Ar injection.

Keywords: GAMMA 10/PDX, E-Divertor, LINDA code, Ar injection, hydrogen injection, plasma detachment

DOI: 10.1585/pfr.13.3403080

1. Introduction

In the future plasma confinement devices such as ITER and DEMO, control of the high heat and particle fluxes on divertor plate is one of the critical issues. The divertor is expected to be exposed to the high heat-load. Chemical and physical sputtering are produced on the divertor plates due to high upstream particle and heat fluxes striking on the target plates [1]. Therefore, it is necessary to protect the plasma facing components (PFCs) from high upstream heat load. The detached plasma regime has been considered as one of the ways to handle the high heat-load on the divertor target plates [2–6]. Radiator gas injection into the plasma edge region is one of the possible ideas to minimize the heat load on the divertor plates because radiator gas strongly enhances the electron power loss channels by increasing radiation power loss and consequently decreases the electron temperature [1–3]. On the other hand, hydrogen atomic and molecular processes play a key role to reduce the ion temperature by enhancing the charge-exchange loss. In addition to these above physical processes, the volume recombination processes such as Molecular Activated Recombination (MAR) [3] and Electron-Ion Recombination (EIR) [13]) are also very much important atomic and molecular processes at the low temperature plasma (< 5 eV) to generate detached plasma.

The 27 m long GAMMA 10/PDX is a linear plasma confinement device, which consists of multiple-cells to confine the plasma [5]. The divertor simulation research (E-Divertor) has been done in GAMMA 10/PDX to clarify the effects of impurity gases on the plasma detachment [5–7]. The E-divertor project has been aimed to investigate the physical mechanism of plasma detachment such as radiation cooling, impurity transport, etc. The generation of a detached plasma has been observed in the D-module due to radiator gas injection into the D-module of GAMMA 10/PDX [5–7]. Simultaneous injection of H and Ar has shown a promising effect on the reduction of ion flux in the case of higher gases injection (a very rough estimation of H and Ar density $\sim 10^{19}$ m^{-3} or more) into the D-module of GAMMA 10/PDX [7]. The plasma detachment state has not been observed in the D-module experiments at the lower impurity injection cases.

Numerical simulation studies have been effectively progressed to reveal the physical mechanism of divertor plasma physics [14–18]. A numerical simulation study is a powerful tool to explain the detailed physical mechanism related to the plasma detachment. The divertor simulation studies have been effectively performed by developing the multi-fluid code and the Monte-Carlo code. The plasma transport in the divertor region has been described by a fluid code while the neutral model can be defined by either

author's e-mail: shahinul@prc.tsukuba.ac.jp
*) This article is based on the presentation at the 26th International Toki Conference (ITC26).

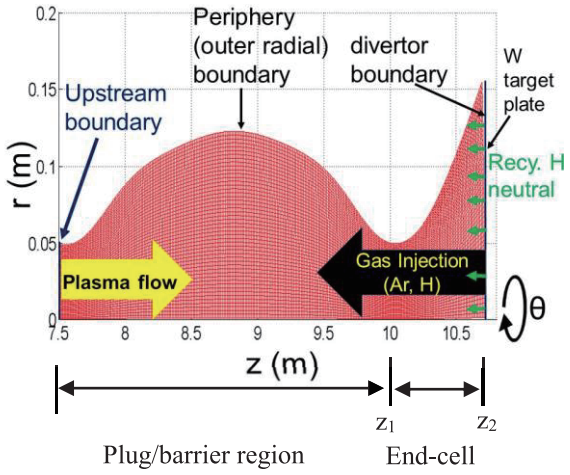

Fig. 1 Mesh structure of the simulation space.

a fluid model or a Monte-Carlo model. A numerical simulation study by using the LINDA (Linear Divertor Analysis with fluid model) code has been performed in the end-cell of GAMMA 10/PDX with a view to explaining the physical mechanism of plasma detachment during neutral gas injection into the E-divertor region [10, 11]. The LINDA code is a multi-fluid code which has been developed based on the same physical models as the B2 code [8]. The detailed effects of magnetic mirror plasma confinement such as plasma trapped in a mirror filed have not yet included in the codes. However, the fluid equations of the codes have been developed with metric of magnetic field, which induces the geometrical configuration of the magnetic field effect in the fluid equations. The fruitful outcomes of theses codes may help us to understand the physical mechanism of plasma-neutral interactions in the divertor region. In the LINDA code, the plasma transport has been modeled by solving the fluid equations while the neutral profile has been modeled by the 1D continuity equation, we are planning to improve the neutral model in the future.

The aim of the paper is to investigate the effects of H and Ar injection into the E-divertor region of GAMMA 10/PDX numerically by using the LINDA code.

2. Simulation Model

In the LINDA code, the mesh structure is designed based on the magnetic field configuration of the GAMMA 10/PDX. Figure 1 shows the mesh structure of the simulation region. As represented in Fig. 1, a tungsten (W) target plate is considered in the simulation space. 321 mesh points are used in the z-axial axis while 50 mesh points are considered in the radial r-axis. Furthermore, the hydrogen plasmas flow out from the upstream region to the downstream region. On the other hand, neutral particles (H, Ar) are transported from downstream to upstream region.

The LINDA code consists of four fluid equations: continuity equation, diffusion equation for the perpendicular direction, momentum balance equation, ion and electron energy balance equations [11]. Continuity equation has been solved only for the ion species while the electron density (n_e) has been assumed to satisfy the relation $n_e = \Sigma\ (i = 1, \ldots, N_\alpha)\ Z_\alpha \times n_\alpha$, (where n_α is the ion density for the charge state of Z_α). The ambipolar flow is assumed in the present LINDA code. The fluid equations of the code are written below:

Continuity equation of ion species α is:

$$\frac{\partial n_\alpha}{\partial t} + \frac{1}{\sqrt{g}}\frac{\partial}{\partial x}\left(\frac{\sqrt{g}}{h_x} n_\alpha u_\alpha\right) \frac{1}{\sqrt{g}}\frac{\partial}{\partial y}\left(\frac{\sqrt{g}}{h_x} n_\alpha v_\alpha\right) = S^\alpha_{\mathrm{n}}. \tag{1}$$

Momentum balance equation of ion species α is:

$$\begin{aligned}
&\frac{\partial}{\partial t}(m_\alpha n_\alpha u_{\|\alpha}) \\
&\quad + \frac{1}{\sqrt{g}}\frac{\partial}{\partial x}\left(\frac{\sqrt{g}}{h_x} m_\alpha n_\alpha u_\alpha u_{\|\alpha} - \eta^\alpha_x \frac{\sqrt{g}}{h_x^2}\frac{\partial u_{\|\alpha}}{\partial x}\right) \\
&\quad + \frac{1}{\sqrt{g}}\frac{\partial}{\partial y}\left(\frac{\sqrt{g}}{h_y} m_\alpha n_\alpha u_\alpha u_{\|\alpha} - \eta^\alpha_x \frac{\sqrt{g}}{h_y^2}\frac{\partial u_{\|\alpha}}{\partial y}\right) \\
&= \frac{1}{h_x}\frac{B_\theta}{B}\left[-\frac{\partial p_\alpha}{\partial x} - \frac{z_\alpha n_\alpha}{n_e}\frac{\partial p_e}{\partial x}\right. \\
&\quad + c_e\left(\frac{z_\alpha}{z_{\mathrm{eff}}} - 1\right) Z_\alpha n_e \frac{\partial T_e}{\partial x} \\
&\quad \left. + c_i\left(\frac{z_\alpha}{z_{\mathrm{eff}}} - 1\right) Z_\alpha n_\alpha \frac{\partial T_i}{\partial x}\right] + \sum_{\beta=1}^{N} F_{\alpha\beta} + S^\alpha_{mu_\|}.
\end{aligned} \tag{2}$$

On the right-hand side, the 1st and the 2nd terms express pressure gradient force. The 3rd and the 4th part correspond to the thermal force for electron and ion, respectively. The 5th term is the friction force. The friction force plays a key role to transport impurity in the plasma upstream direction. The last term on the right-hand side of equation (2) is the source and sink terms for the plasma.

Diffusion approximation in the radial direction is:

$$v_\alpha = -\frac{1}{h_y} D^\alpha_{\mathrm{n}} \frac{\partial}{\partial y}(\ln n_\alpha). \tag{3}$$

The ion energy balance equation:

$$\begin{aligned}
&\frac{\partial}{\partial t}\left(\frac{3}{2} n_i T_i + \sum\nolimits_\alpha \frac{1}{2}\rho_\alpha u^2_{\|\alpha}\right) \\
&\quad + \frac{1}{\sqrt{g}}\frac{\partial}{\partial x}\left[\frac{\sqrt{g}}{h_x}\left(\sum\nolimits_\alpha \frac{5}{2} n_\alpha u_\alpha T_i + \sum\nolimits_\alpha \frac{1}{2} m_\alpha n_\alpha u_\alpha u^2_{\|\alpha}\right)\right. \\
&\quad \left. - \frac{\sqrt{g}}{h_x^2}\left(\kappa^i_x \frac{\partial T_i}{\partial y} + \sum\nolimits_\alpha \frac{1}{2}\eta^\alpha_x \frac{\partial u^2_{\|\alpha}}{\partial x}\right)\right] \\
&\quad + \frac{1}{\sqrt{g}}\frac{\partial}{\partial y}\left[\frac{\sqrt{g}}{h_y}\left(\sum\nolimits_\alpha \frac{5}{2} n_\alpha v_\alpha T_i + \sum\nolimits_\alpha \frac{1}{2} m_\alpha n_\alpha v_\alpha u^2_{\|\alpha}\right)\right. \\
&\quad \left. - \frac{\sqrt{g}}{h_y^2}\left(k^i_y \frac{\partial T_i}{\partial y} + \sum\nolimits_\alpha \frac{1}{2}\eta^\alpha_y \frac{\partial u^2_{\|\alpha}}{\partial y}\right)\right] \\
&= -\frac{u_e}{h_x}\frac{\partial p_e}{\partial x} - \frac{v_e}{h_y}\frac{\partial p_e}{\partial y} + k(T_e - T_i) \\
&\quad + S^i_E + \sum\nolimits_{\alpha\beta} F_{\alpha\beta}(u_{\|b} - u_{\|\alpha}).
\end{aligned} \tag{4}$$

The electron energy balance equation:

$$\frac{\partial}{\partial t}\left(\frac{3}{2}n_{\mathrm{e}}T_{\mathrm{e}}\right)+\frac{1}{\sqrt{g}}\frac{\partial}{\partial x}\left(\frac{\sqrt{g}}{h_x}\frac{5}{2}n_{\mathrm{e}}u_{\mathrm{e}}T_{\mathrm{e}}-\kappa_x^{\mathrm{e}}\frac{\sqrt{g}}{h_x^2}\frac{\partial T_{\mathrm{e}}}{\partial x}\right)+\frac{1}{\sqrt{g}}\frac{\partial}{\partial y}\left(\frac{\sqrt{g}}{h_y}\frac{5}{2}n_{\mathrm{e}}v_{\mathrm{e}}T_{\mathrm{e}}-\kappa_y^{\mathrm{e}}\frac{\sqrt{g}}{h_y^2}\frac{\partial T_{\mathrm{e}}}{\partial y}\right)=\frac{u_{\mathrm{e}}}{h_x}\frac{\partial p_{\mathrm{e}}}{\partial x}+\frac{v_{\mathrm{e}}}{h_y}\frac{\partial p_{\mathrm{e}}}{\partial y}-k(T_{\mathrm{e}}-T_{\mathrm{i}})-k_{\mathrm{z}}(T_{\mathrm{e}}-T_{\mathrm{z}})+S_{\mathrm{E}}^{\mathrm{e}}. \tag{5}$$

On the right-hand side, the 1st and the 2nd term are the pressure gradient force. The 3rd and the 4th term correspond to the energy exchange between electron-ion, and electron-neutral, respectively. The last term represents source and sink terms for the electron.

The following notification are used in the above equations: n_{e} and n_{i} represent the electron and ion density, g, h_x and h_y represent the metrics terms, v_{e} is the velocity of electron, m_α and Z_α are the mass and charge number of species α, T_{e} and T_{i} represent the temperature of electron and ion, T_z is the temperature of impurity ion (0.0259 eV), P_{e} is the pressure of electrons, u is the flow velocity, B and B_θ are the magnetic induction and the component of magnetic field, $F_{\alpha\beta}$ is the friction force between species α and β, Z_{eff} is the effective charge, η and κ represent the viscosity coefficient and thermal conductivity, c_{e} and c_{i} are the coefficients of thermal force, D_{n}^{α} is the Bohm diffusion constant. S_{n}^{α}, $S_{mu\|}^{\alpha}$, $S_{\mathrm{E}}^{\mathrm{e}}$, $S_{\mathrm{E}}^{\mathrm{i}}$, represent the volume source of particles, parallel momentum, electron and ion energy due to interactions of plasma with the neutral particles. In the LINDA code, the interactions between charged and neutral particles for ions and electron are include in the source terms of the equations. The source and sink terms of the LINDA code are written below:

$$S_{\mathrm{n}}=n_0n_{\mathrm{e}}\langle\sigma v\rangle_{\mathrm{ionz.}}-n_{\mathrm{e}}n_{\mathrm{i}}\langle\sigma v\rangle_{\mathrm{rec.}}+n_{\mathrm{e}}n_z\langle\sigma v\rangle_{\mathrm{ioni\text{-}z.}}-n_{\mathrm{e}}n_{\mathrm{imp}}\langle\sigma v\rangle_{\mathrm{z\text{-}rec.}}, \tag{6}$$

$$S_{mu\|}=-n_0n_{\mathrm{i}}\langle\sigma v\rangle_{\mathrm{cx}}m_{\mathrm{i}}(u_{\mathrm{i}}-u_{\mathrm{n}})-n_{\mathrm{e}}n_{\mathrm{i}}\langle\sigma v\rangle_{\mathrm{rec.}}m_{\mathrm{i}}u_{\mathrm{i}}, \tag{7}$$

$$S_{\mathrm{E}}^{\mathrm{i}}=n_0n_{\mathrm{e}}E_{\mathrm{n}}\langle\sigma v\rangle_{\mathrm{ionz.}}-n_{\mathrm{n}}n_{\mathrm{i}}\langle\sigma v\rangle_{\mathrm{CX}}(0.5m_{\mathrm{i}}u_{\mathrm{i}}^2+T_{\mathrm{i}}-E_{\mathrm{n}})-n_{\mathrm{e}}n_{\mathrm{i}}\langle\sigma v\rangle_{\mathrm{rec.}}(T_{\mathrm{i}}+0.5m_{\mathrm{i}}u_{\mathrm{i}}^2), \tag{8}$$

$$S_{\mathrm{E}}^{\mathrm{e}}=-n_0n_{\mathrm{e}}\langle\sigma v\rangle_{\mathrm{ionz.}}L_{\mathrm{e}}-n_{\mathrm{e}}n_{\mathrm{i}}\langle\sigma v\rangle_{\mathrm{rec.}}T_{\mathrm{e}}-n_{\mathrm{e}}n_zL_z-n_{\mathrm{e}}n_{\mathrm{imp}}\langle\sigma v\rangle_{\mathrm{z\text{-}rec.}}T_{\mathrm{e}}, \tag{9}$$

where, L_{e} (25 eV) includes the loss of electron energy during ionization and radiation loss of H atom [8], L_z is the radiative cooling rate of impurity particles [12], $E_{\mathrm{n}}=0.5mu_{\mathrm{n}}^2$ is the neutral energy, n_{imp} is the impurity ion density, n_0 and n_z are the hydrogen and impurity neutral density, respectively.

The upstream boundary conditions are applied in front of the most left side of Fig. 1. The upstream boundary conditions are fixed during iterations. During the iteration process, the upstream boundary conditions are given below:

Electron heat flux,

$$F_{\mathrm{e}}(z=0,r,N_{\mathrm{it}})=\frac{5}{2}n_{\mathrm{e}}T_{\mathrm{e}}u_{\mathrm{i}}. \tag{10}$$

Ion heat flux,

$$F_{\mathrm{i}}(z=0,r,N_{\mathrm{it}})=\frac{5}{2}n_{\mathrm{i}}T_{\mathrm{i}}u_{\mathrm{i}}. \tag{11}$$

Particle flux,

$$\Gamma_{\mathrm{i}}(z=0,r,N_{\mathrm{it}})=n_{\mathrm{i}}u_{\mathrm{i}}. \tag{12}$$

At the initial stage of iteration, the initial conditions of the plasma parameters are given based on the following four equations:

$$n_{\mathrm{i}}(z,r,N_{\mathrm{it}}=1)=5\times10^{18}\times\mathrm{e}^{-\frac{1}{2}\left\{\frac{r}{r_{0\mathrm{n}}(z)}\right\}^2}, \tag{13}$$

$$T_{\mathrm{i}}(z,r,N_{\mathrm{it}}=1)=100\times\mathrm{e}^{-\frac{1}{2}\left\{\frac{r}{r_{0\mathrm{i}}(z)}\right\}^2}, \tag{14}$$

$$T_{\mathrm{e}}(z,r,N_{\mathrm{it}}=1)=30\times\mathrm{e}^{-\frac{1}{2}\left\{\frac{r}{r_{0\mathrm{e}}(z)}\right\}^2}, \tag{15}$$

$$u_{\mathrm{i}}(z,r,N_{\mathrm{it}}=1)=\frac{1}{2}\sqrt{\frac{n_{\mathrm{e}}T_{\mathrm{e}}+n_{\mathrm{i}}T_{\mathrm{i}}}{m_{\mathrm{i}}n_{\mathrm{i}}}}. \tag{16}$$

Where, $r_{0\mathrm{n}}$, $r_{0\mathrm{i}}$, $r_{0\mathrm{e}}$ indicate half maximum full-width of physical quantities, r is spatial position of physical quantities in the radial direction, N_{it} is the number of iteration. The values of the half maximum full-width are given based on the typical experimental parameters of GAMMA 10/PDX. Neumann boundary condition has been applied on the periphery region (outer radial boundary). The periphery boundary of plasma parameters is written as follows:

$$X/\left(\frac{\mathrm{d}X}{\mathrm{d}r}\right)=\text{const.} \tag{17}$$

Where, $X=n_{\mathrm{i}}$, T_{i}, T_{e}.

Furthermore, the divertor boundary conditions for the ion and the electron energy equations have been applied on the tungsten target plate. The Bohm condition near the sheath entrance has been considered in the LINDA code. The hydrogen ion parallel velocity near the sheath entrance is represented by the following equation:

$$u_{\mathrm{i}\|}=\sqrt{\frac{T_{\mathrm{i}}+T_{\mathrm{e}}}{m_{\mathrm{i}}}}. \tag{18}$$

The heat transmission coefficients through the sheath entrance have been defined as follows:

The ion heat transfer coefficient:

$$\alpha_{\mathrm{i}}=2\frac{T_{\mathrm{i}}}{T_{\mathrm{e}}}. \tag{19}$$

The electron heat transfer coefficient:

$$\alpha_{\mathrm{e}}=\frac{2}{1-\delta_{\mathrm{e}}}-\frac{1}{2}\ln\left\{\left(2\pi\frac{m_{\mathrm{e}}}{m_{\mathrm{i}}}\right)\left(1+\frac{T_{\mathrm{i}}}{T_{\mathrm{e}}}\right)(1-\delta_{\mathrm{e}})^{-2}\right\}. \tag{20}$$

The boundary conditions for the electron (q_{e}) and ion (q_{i}) energy balance equations on the target plate are as follows:

$$q_{\mathrm{i}}=\alpha_{\mathrm{i}}n_{\mathrm{i}}u_{\mathrm{i}\|}T_{\mathrm{i}},\quad q_{\mathrm{e}}=\alpha_{\mathrm{e}}n_{\mathrm{e}}u_{\mathrm{e}\|}T_{\mathrm{e}}. \tag{21}$$

The heat flux and particle flux on the target plate are:

$$\text{Heat flux, } q=q_{\mathrm{i}}+q_{\mathrm{e}}. \tag{22}$$

$$\text{Particle flux, } \Gamma_{\mathrm{i}}=n_{\mathrm{i}}u_{\mathrm{i}\|}. \tag{23}$$

Where, m_i and m_e are the mass of proton and electron, respectively, δ_e is coefficient of secondary electron emission, $u_{e\|}$ is the electron parallel velocity. In addition, the flux limits for the parallel viscosity and electron thermal conductivity have been introduced in the LINDA code according to the B2 and B2.5 code [8, 9]. The classical transport coefficients have been considered for the parallel direction while the anomalous transport coefficients have been used in the radial direction. In the LINDA code, the hydrogen atomic processes (CX, ionization and recombination) and Ar processes (ionization, radiation cooling and recombination) have been considered in order to study plasma-neutral interactions [12]. At the current stage, the neutral profile has been given by solving the 1D continuity equation, since the precise neutrals profile are not needed at present. In the present study, simplified neutral models have been used. The neutral profile has been calculated iteratively together with the fluid equations.

In this study, the H and Ar neutral models are given analytically by solving 1D continuity equations. As for the hydrogen neutral model, the injected neutral density assumed to be uniform in the mirror throat region ($z \sim 10.3$ m) and reduces exponentially along the upstream region. The radial profile is assumed to be uniform. The hydrogen neutral model is written as follows

$$n_O(z) = n_r \exp\left\{-\int_z^{z_1} \frac{dz}{\lambda_{rec}(z)}\right\} + n_{0H} \exp\left\{-\int_z^{z_1} \frac{dz}{\lambda_H(z)}\right\}, \quad (24)$$

$$n_O(z) = n_r \exp\left\{-\int_z^{z_2} \frac{dz}{\lambda_{rec}(z)}\right\} + n_{0H}. \quad (25)$$

The recycling hydrogen neutral density (n_r) and velocity (u_n) on the target plate are written as follows:

$$n_r = R_N \frac{n_i u_{i\|}}{u_n}, \quad (26)$$

$$u_n = \sqrt{\frac{\left(\frac{R_E}{R_N} \times T_{i,target}\right)}{m_i}}. \quad (27)$$

Where, $z_2 = 10.705$, $z_1 = 10.045$, n_O represents the hydrogen neutral density, n_r represents the recycling H neutral density, $\lambda_{rec} = \frac{u_n}{n_e\langle\sigma v\rangle_{cx} + n_e\langle\sigma v\rangle_{ionz}}$ represents the recycling neutral mean free path, n_{0H} is the injected hydrogen neutral density, $\lambda_H = \frac{\sqrt{3/m_i}}{n_e\langle\sigma v\rangle_{cx} + n_e\langle\sigma v\rangle_{ionz}}$ is the injected hydrogen neutral mean free path, the temperature of injected hydrogen atom is assumed to be the Frack-Condon energy 3 eV, $\langle\sigma v\rangle_{cx}$ and $\langle\sigma v\rangle_{ionz}$ are the reaction rate coefficient for CX ($H^+ + H^0 \rightarrow H^0 + H^+$) and ionization ($H^0 + e \rightarrow H^+ + 2e$) [12], R_N and R_E are the particle and energy reflection coefficient, respectively [1], $n_i u_{i\|}$ represents the hydrogen ion flux on the target plate.

Equation (24) describes hydrogen neutral density in the plug/barrier region (7.5 m $\leq z \leq$ 10.045 m) while equation (25) describes hydrogen neutral density in the end-cell (10.055 m $\leq z \leq$ 10.705 m). The z-axial profile of hydrogen neutral particles along the z-axis has been shown in Fig. 2 (a). The increase in the H neutral profile near the target plate is observed, which represents the contribution recycling H neutral by the target plate. The distribution of Ar neutral density is assumed to be uniform in the end-cell (10.055 m $\leq z \leq$ 10.705 m) while reduces exponentially in the plug/barrier region (7.50 m $\leq z \leq$ 10.045 m). The z-axial profile of Ar neutral particles is also shown in Fig. 2 (b). The distribution of Ar neutral particles along the radial axis is assumed to be uniform. The Ar neutral model in the plug/barrier region is given by the following formula,

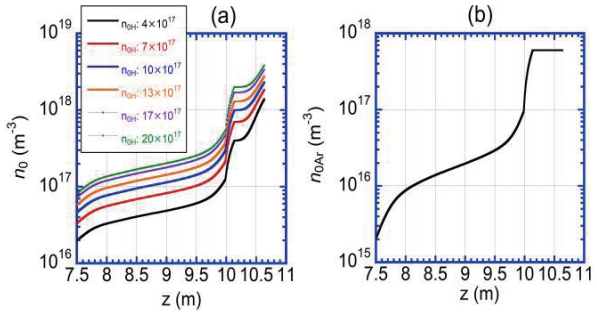

Fig. 2 Distribution of neutral particles on the z-axis (a) H and (b) Ar in the case of injected neutral: 6×10^{17} m^{-3}.

$$n_{Ar}(z) = n_{Ar\text{-}in} \exp\left\{-\int_z^{z_1} \frac{dz}{\lambda_{Ar}(z)}\right\}. \quad (28)$$

Where, n_{Ar} is the Ar neutral density, $n_{Ar\text{-}in}$ is the injected Ar neutral density and $\lambda_{Ar} = \frac{\sqrt{0.0259/m_z}}{n_e\langle\sigma u\rangle_{ioni-z}}$ is the mean free path of Ar neutral particles, $\langle\sigma u\rangle_{ioni-z}$ is the ionization reaction rate coefficient of Ar neutral particles [12]. The temperature of the impurity particles is assumed to be room temperature (0.0259 eV). The decay of the neutral particles (Ar and H) is assumed to be steep around $z \sim 10.1$ m, because in these regions the plasma density is high due to the particle balance (flux tube contraction).

3. Simulation Results and Discussion

In this simulation, the injected Ar density has been fixed at 6×10^{17} m^{-3}, while the injected hydrogen neutral atom density has been varied from 0.0 to 2.8×10^{18} m^{-3}. The simulation outcomes are shown in Figs. 3 to 5. The 2-dimensional profiles of the electron and ion temperature are plotted in Fig. 3. A slight reduction in the temperature near the target plate is shown in Fig. 3 (a) for without any gas injection. The recycling hydrogen neutrals are included in the present study. Due to the above, reduction in the temperature is observed near the target. Furthermore, the reduction rate has been enhanced when hydrogen gas is artificially injected as shown in Figs. 3 (b) and (c). Moreover, a noticeable reduction in the ion temperature has been shown with the increasing H injection as shown in Fig. 3 (c) left-side. The electron temperature also reduces according to the increasing H injection into the end-cell as plotted in Fig. 3 (c) right-side.

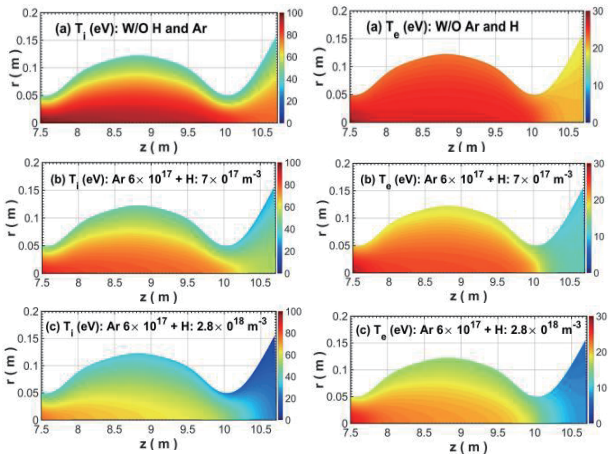

Fig. 3 2D profiles of the ion (left-side) and electron (right-side) temperature (a) W/O gas (b) simultaneous injection of H 7.0×10^{17} m^{-3} and Ar (c) simultaneous injection of H 2.8×10^{18} m^{-3} and Ar.

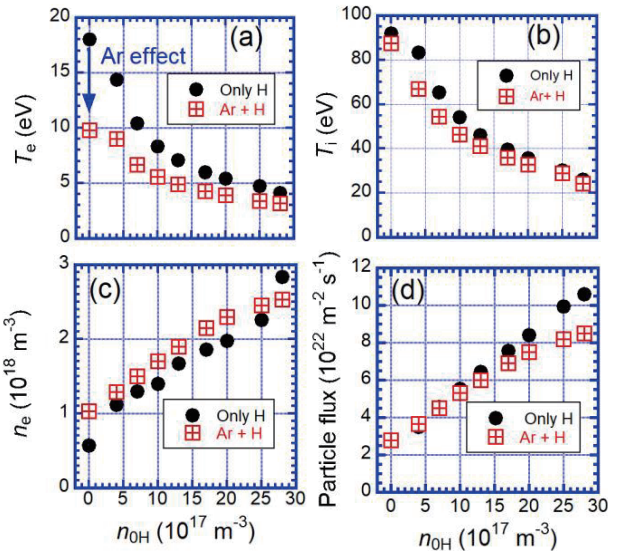

Fig. 4 Dependence of plasma parameters on the target plate (at $r = 0$ cm) (a) electron temperature (b) ion temperature (c) electron density and (d) particle flux of H as a function of the injected H neutral density in the cases of simultaneous injection of Ar and H, Ar density is fixed at 6×10^{17} m^{-3}.

The dependence of the electron temperature (T_e) on the target plate (at $r = 0$ cm) against the injected hydrogen neutral density has been plotted in Fig. 4 (a). The black circle represents data for only H injection while the red square represents data for simultaneous injection of Ar and H. In this case, the Ar density is fixed at 6×10^{17} m^{-3} and H is varied (Ar + H). For only Ar 6×10^{17} m^{-3} injection ($n_{0H} = 0$), the T_e on the target plate decreases to nearly 10 eV, which indicates the radiation cooling effects of Ar neutral particles. On the other hand, for only H 4×10^{17} m^{-3} injection, the T_e on the target plate decreases to nearly 14 eV. The T_e also decreases with the increasing H injection. For the only strongest H injection, the T_e on the target plate decreases to nearly 4.5 eV. It is shown that the reduction in the T_e for simultaneous injection of H and Ar is higher than that of only H injection. In this case, for the strongest H injection T_e on the target plate reduces to about 3.2 eV.

The dependence of ion temperature (T_i) on the target plate against the H neutral density is also plotted in Fig. 4 (b). The reduction rate of ion temperature is almost similar for only H injection and simultaneous injection of Ar and H. However, a slight influence of Ar injection on the ion temperature has been observed in the range of low hydrogen density ($< 1.3 \times 10^{18}$ m^{-3}). For the strongest H injection, T_i on the target plate reduces to about 25 eV.

The dependence of electron density (n_e) on the target plate has been also plotted in Fig. 4 (c). The electron density increases with the increasing H injection. It is recognized that n_e is higher for the simultaneous injection of Ar and H than that of only H injection, which indicates ionization effects of Ar neutral particles. During the simultaneous injection of Ar and H, the electron density becomes saturated at the H injection of 2.5×10^{18} m^{-3}. On the other hand, for only H injection, the electron density continues to increase with the increasing H injection. The ionization reaction rate reduces according to the reduction of electron temperature. The reduction in the electron temperature is larger for simultaneous injection of Ar and H comparing to only H injection, which induces a saturation in the electron density in the case of simultaneous injection of Ar and H.

Figure 4 (d) represents the dependence of hydrogen ion particle flux (Γ_i) on the target plate as a function of the injected H neutral density. At the lower H gas injection region, the particle flux is almost similar for simultaneous injection of Ar and H compared with the only H injection. However, the tendency has been changed according to increasing H neutral density. During the simultaneous injection of Ar and H, the particle flux becomes saturated at the H injection of 2.5×10^{18} m^{-3}. On the other hand, for only H injection, the particle flux continues to increase according to the increasing H injection.

The energy loss processes have also been investigated to explore the physical mechanism related to the plasma energy loss processes during neutral injection. The dependence of the CX (charge-exchange) loss ($H^+ + H^0 \rightarrow H^0 + H^+$) and recombination loss ($H^+ + e \rightarrow H$) as a function of the injected hydrogen neutral density is plotted in Fig. 5 (a). The CX loss increases significantly during H injection. As a result, the ion temperature significantly reduces via the CX loss as shown in Fig. 4 (b). Furthermore, the CX loss increases with the increasing hydrogen injection. The CX reaction rate coefficient ($\langle \sigma v \rangle$) is almost a nearly flat profile in the temperature range from 10 eV to 100 eV [12]. Therefore, the CX loss strongly depends on the proton and hydrogen neutral density. Because of this, CX loss increases with the increasing neutral density, although the ion temperature is reduced with the increasing hydrogen neutral density. Furthermore, the significant effect of Ar injection on the CX loss has not been

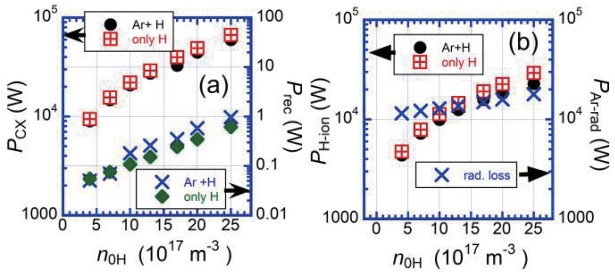

Fig. 5 Dependence of (a) CX loss and recombination loss, and (b) ionization loss and Ar radiative loss as a function of H neutral density.

observed, since Ar neutral particle has no direct effect on the CX loss mechanism. The recombination loss is small. However, the recombination loss increases as the electron temperature is reduced. The recombination processes become active in the low temperature region ($T_e < 1$ eV). In this study, T_e reduces to about 3 eV. The ionization reaction rate coefficient ($\langle\sigma v\rangle$) is comparatively higher than that of the recombination rate coefficient ($\langle\sigma v\rangle$) in the 3 eV range [12]. As shown in Fig. 5 (b), the power loss for the ionization of hydrogen neutral particles increases with the increasing H neutral density. It is shown that ionization loss is slightly high for only H injection compared to the simultaneous injection of Ar and H. The ionization reaction rate coefficient ($\langle\sigma v\rangle$) strongly depends on the electron temperature [12]. The electron temperature reduction is higher for combined injection of Ar and H than that of only H injection. As a result, the ionization power loss is low for combined injection of Ar and H than that of only H injection. The radiation power loss depends on the electron density, Ar density and radiation power loss function (L_Z). The radiation power loss function decreases with the decreasing electron temperature [12]. However, the electron density increases with the increasing H injection. As a result, the radiation power loss shows a slight dependence on the injected hydrogen neutral density.

The effect of recycling molecules is not included in the present LINDA code. In addition, the LINDA code has not yet considered the effect of the hydrogen ion acceleration by the sheath potential on the neutral atoms reflected from the target plate and of the fast neutral hydrogen atoms produced by the CX reaction. The mean free path (MFP) and the neutral distribution profile may be changed if the above physical processes are included in the present LINDA code. In addition to the above processes, the effects of mirror magnetic trap has not also included in the LINDA code so far. It is our future plan to include the mirror magnetic effect in the LINDA code.

4. Summary

In this study, effects of Ar and H injection into the end-cell of GAMMA 10/PDX have been investigated numerically by using the multi-fluid code "LINDA". Hydrogen injection in the end-cell reduces the ion temperature significantly by increasing the CX loss. The CX loss increases with the increasing H injection. The electron temperature reduces during Ar injection. Reduction in the electron temperature is larger for simultaneous injection of Ar and H than that of only H injection. For the simultaneous injection of H and Ar, the electron density and the particle flux shows a tendency of saturation at the higher H injection, which implies that the plasma in the end-cell approaches the plasma detachment state. The tendency of saturation in the electron density and particle flux have not been shown for only H injection. The significant effect of Ar injection on the CX, ionization and recombination loss has not been observed in the study.

In the future works, we will describe the hydrogen neutral profile by developing a kinetic neutral code. We will try to include detailed MAR processes [19] in the kinetic neutral code. We plan to couple the neutral kinetic code with the present LINDA code to evaluate and discuss the detailed MAR processes and its effects on the plasma detachment. We will also try to design a V-shape target at the end of the mesh to simulate realistic divertor simulation experiment of GAMMA 10/PDX. We plan to compare the LINDA code with the other similar code in the future. Finally, we will validate E-divertor experiment results with the LINDA code.

Acknowledgements

This study was supported by the bidirectional collaboration research program of the University of Tsukuba, Keio University, and National Institute for Fusion Science (NIFS12KUGM066, NIFS14KUGM086). The author would like to thank the members of the GAMMA 10 group.

[1] P.C. Stangeby, Plasma Phys. Control. Fusion **43**, 223 (2000).
[2] A. Loarte *et al.*, Nucl. Fusion **47**, S203 (2007).
[3] S.I. Krasheninkov *et al.*, Phys. Plasma **23**, 055602 (2016).
[4] N. Ohno, Plasma Phys. Control. Fusion **59**, 034007 (2017).
[5] Y. Nakashima *et al.*, Nucl. Fusion **57**, 116033 (2017).
[6] M.S. Islam *et al.*, Plasma Fusion Res. **11**, 2402042 (2016).
[7] Y. Nakashima *et al.*, J. Nucl. Mater. **463**, 537 (2015).
[8] B.J. Braams, NET Rep. 68 EURFU/X-80/87/68, CEC, Brussels (1987).
[9] R. Schneider *et al.*, Contrib. Plasma Phys. **46**, 3 (2006).
[10] M.S. Islam *et al.*, Fusion Eng. Des. **125**, 216 (2017).
[11] M.S. Islam *et al.*, Plasma Phys. Control. Fusion **59**, 125010 (2017).
[12] D.E. Post *et al.*, J. Nucl. Mater. **220**, 143 (1995).
[13] Y. Hahn, Rep. Prog. Phys. **60**, 691 (1997).
[14] K. Hoshino *et al.*, Plasma Fusion Res. **12**, 1405023 (2017).
[15] X.J. Liu *et al.*, Phys. Plasmas **24**, 122509 (2017).
[16] X. Bonnin *et al.*, Nucl. Mater. Energy **12**, 1100 (2017).
[17] Y. Feng, Plasma Phys. Control. Fusion **59**, 034006 (2017).
[18] G. Kawamura *et al.*, Plasma Fusion Res. **5**, S1020 (2010).
[19] K. Miyamoto *et al.*, J. Phys. Soc. Jpn. **76**, 034501 (2007).